Modelling and Control of Non-Isolated High Voltage Gain Boost Converter Employing Coupled Inductor and Switched Capacitor

M. Muhammad, M. Armstrong, M. A. Elgendy.
School of Electrical Electronic Engineering Newcastle University
Newcastle upon Tyne, United Kingdom
m.muhammad@ncl.ac.uk, matthew.armstrong@ncl.ac.uk

***Abstract*—This paper investigates mathematical model of a high gain step-up boost converter built around coupled inductor and switched capacitor. Unlike the classical boost converter, which transfers input power to the output during the switch OFF period, here power is transferred to the output during the switch ON period. A state space averaging method is employed to derive the small signal ac model with ideal components. The control to output transfer function exhibits a non-minimum phase system identical to the conventional boost converter. The derived model is validated via simulation. A dual loop average current mode controller is designed to regulate the converter output voltage. Experimental results taken from a 250W laboratory prototype operating with an input voltage of 20V and output voltage of 190V verify the effectiveness of the controller. The proposed converter is well suited for renewable energy and grid connected power system applications.**

Keywords—High step-up DC-DC Converter Modelling, Control design, Coupled Inductor and Switched Capacitor.

I. INTRODUCTION

Many application involving power electronic converters requires the regulation of either the input voltage/current or output voltage/current of the power converter. For example, in solar photovoltaic (PV) pumping applications the input voltage of the converter is controlled to track the maximum power point of the PV modules [1-3]. Similarly, in a grid connected inverter systems, the output current can be controlled using advanced techniques to improve power quality performance, or eliminate DC current injection in transformerless systems[4],[5].

In distributed power generation system [6], specific dc-dc power electronics converters with regulated input current or output voltage are required to meet the requirement of various local loads before interconnection with the utility grid and/ or onward supply to consumer loads. Proton exchange membrane (PEM) fuel cell (FC) systems are widely used in conjunction with auxiliary energy storage system (ESS) in electric vehicles [7]. The practical implementation of a FC powered vehicle requires a dc-dc power converter to boost the low voltage FC stack output voltage to the rated load voltage. Various converter topologies have been proposed depending on the application. A possible solution is to use conventional boost or buck-boost converters that step-up the voltage and allow easy control of converter input/output current and output voltage. The main drawback of classical non-isolated boost or buck-boost converters is extreme duty operation and its lower efficiency when operating under steep input-output voltage transfer ratio.

In many modern applications, such as uninterruptible power supply (UPS) [8], battery charging and discharging [9], electric vehicles [10] and motor control [11], a dc-dc converter is used as an interface to produce a regulated output voltage from unregulated source. The ratio of input voltage to output voltage can often be considerable. Depending on the magnitude of the source voltage, a high step-up dc-dc converter is required to raise the source voltage to match the requirement of the load.

This paper presents modelling and control design of the high step dc-dc boost converter topology proposed in [12]. The converter adopts coupled inductor and switched capacitor to achieve high conversion ratio; whilst minimizing the semiconductor device stress typically observed in power converters of a similar type. This topology is chosen because of its distinct operational characteristics of transferring the input power to the output during switch ON period due to its configuration, and suitability to connect PV system to the network via module integrated inverters. Converter dynamics are discussed in details and proper control is design accordingly using dual loop current mode control.

II. CONVERTER DESCRIPTION AND ANALYSIS

Fig. 1 shows the circuit of the considered high step-up converter highlighting the model of the coupled inductor as an ideal transformer in parallel with magnetizing inductor L_m and in series with leakage inductance L_{Lk} [12-14]. V_{in}, V_O denotes the input and output voltages of the converter respectively and R_O represent the resistive load. The converter comprises a coupled inductor and switch S. The coupled inductor serves two purposes: energy storage and voltage extension, theoretically minimizing the magnetic components count. The primary and secondary windings are denoted by n_1, n_2 and the coupling references denoted by ''*''. The primary winding n_1 is coupled to the corresponding secondary winding n_2. The input side is connected to the clamp capacitor C_C via a clamp diode D_C and this combination is called passive clamp circuit for recycling the leakage inductance energy. The voltage extension cell comprises the clamp diode D_C, the clamp capacitor C_C, the switched capacitor C_m and the secondary

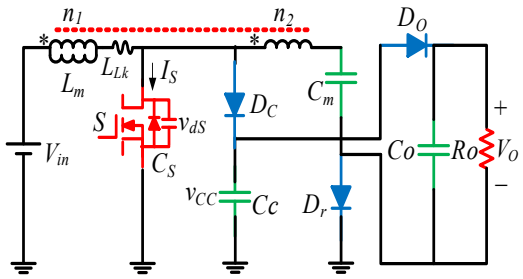

Fig. 1 Considered High step-up converter circuit

winding of the coupled inductor. The output voltage of the converter during the switch ON instant is given by

$$V_O = V_{Cm} + V_{Cc} + NV_{in} \tag{1}$$

During the switch OFF instant, the voltage across the clamp and switched capacitor is denoted by

$$V_{Cc} = V_{in}/(1-D) \tag{2}$$

$$V_{Cm} = N(V_{Cc} - V_{in}) + V_{Cc} \tag{3}$$

Using (1), neglecting the leakage inductance effect and assuming the voltage across all the capacitors to be constant, the voltage gain of the converter can be expressed as

$$M = \frac{V_O}{V_{in}} = \frac{N+2}{(1-D)} \tag{4}$$

Where D is the converter duty cycle and N is the coupled inductor turns ratio.

III. Small Signal Modelling

As previously explained, the converter operation is divided into two subintervals (switch ON and OFF instances). During each interval, the converter equations are derived and can be written in state space model form

$$\dot{x} = A_i x + B_i u \qquad i = 1,2 \tag{5}$$

The state vector is defined as

$$x = [i_{Lm}\ v_{Cc}\ v_{Cm}\ v_O]' \tag{6}$$

And the input is defined as

$$u = [V_{in}] \tag{7}$$

The average model of the circuit in Fig.1 can be developed by averaging the state equations of the ON-period and OFF-period (neglecting short operating intervals). The converter is assumed to operate in a continuous conduction mode (CCM). During the switch ON instant one get the following equations

$$\begin{cases} L_m \dfrac{di_{Lm}}{dt} = v_{in} \\ C_C \dfrac{dv_{Cc}}{dt} = \dfrac{i_{Lm}}{N} \\ C_m \dfrac{dv_{Cm}}{dt} = -\dfrac{i_{Lm}}{N} \\ C_O \dfrac{dv_O}{dt} = \dfrac{v_O - v_{cm} - v_{Cc} - Nv_{in}}{NL_K} - \dfrac{v_O}{R_O} \end{cases} \tag{8}$$

And the equation of the OFF state is given by

$$\begin{cases} L_m \dfrac{di_{Lm}}{dt} = v_{in} - v_{Cc} \\ (N+1)L_m \dfrac{di_{Lm}}{dt} = v_{in} - v_{Cm} \\ C_C \dfrac{dv_{Cc}}{dt} = i_{Lm} - (N+1)\dfrac{v_{cm} - Nv_{in} - (N+1)v_{Cc}}{NL_K} \\ C_m \dfrac{dv_{Cm}}{dt} = \dfrac{i_{Lm}}{(N+1)} \\ C_O \dfrac{dv_O}{dt} = -\dfrac{v_O}{R_O} \end{cases} \tag{9}$$

Using the state space average method in [14], the state space equations that describe the converter dynamics are given by

$$\begin{cases} \langle \dfrac{di_{Lm}}{dt} \rangle = \dfrac{v_{in}}{L_m} - \dfrac{v_{Cc}d'}{L_m} \\ \langle \dfrac{di_{Lm}}{dt} \rangle = -\dfrac{d'v_{Cm}}{(N+1)L_m} + \dfrac{(1+Nd)v_{in}}{(N+1)L_m} \\ \langle \dfrac{dv_{Cc}}{dt} \rangle = \dfrac{i_{Lm}(1-d)}{NC_C d} - \dfrac{v_{in}(N+2)^2(N+1)}{C_C(d\cdot R_o + (N+dN)NL_K)} \\ C_m \langle \dfrac{dv_{Cm}}{dt} \rangle = \dfrac{i_{Lm}d'}{(N+1)} - \dfrac{i_{Lm}d}{N} \\ \langle \dfrac{dv_O}{dt} \rangle = \dfrac{(NL_K(N+dN) + dR_o)d'v_o}{NL_K C_o R_o d} - \dfrac{v_{in}(N+2)}{NL_K C_o} \end{cases} \tag{10}$$

Where $d' = (1-d)$

A. Steady State

The state space averaged DC model that describe the converter in equilibrium is obtained by letting the left-hand side (LHS) of (10) equal to zero, from which

$$\mathrm{X} = -A^{-1}BU \tag{11}$$

And the set of attainable equilibrium points are

$$\times = \begin{bmatrix} I_{Lm} \\ V_{Cc} \\ V_{Cm} \\ V_O \end{bmatrix} = \begin{bmatrix} \dfrac{(N+1)\cdot(N+2)^2\cdot V_{in}\cdot D}{(1-D)\cdot(D\cdot R_o + (N+DN)N\,L_K)} \\ V_{in}/(1-D) \\ (1+Nd)V_{in}/(1-D) \\ \dfrac{(N+2)\cdot V_{in}\cdot R_o\cdot D}{(1-D)\cdot(D\cdot R_o + (N+DN)\cdot N\cdot L_K)} \end{bmatrix} \tag{12}$$

From (12), the steady state voltage gain of the converter considering the leakage inductance is given by

$$\frac{V_O}{V_{in}} = \frac{(N+2)\cdot R_o\cdot D}{(1-D)\cdot(D\cdot R_o + (N+DN)\cdot N\cdot L_K)} \tag{13}$$

B. Perturbation and Linearization

A linearized system can be developed by introducing perturbation around the steady state value of the averaged model calculated in (10), containing the steady state dc value represented by uppercase letter and a superimposed ac variation represented by lowercase symbol with circumflex. For instance the perturbation definitions for the state variable

are: $i_{Lm} = I_{Lm} + \hat{\imath}_{Lm}$, $v_{in} = V_{in} + \hat{v}_{in}$, $v_o = V_o + \hat{v}_o$ and $d = D + \hat{d}$. The following expressions are obtained

$$\begin{cases} L_m \dfrac{d(I_{Lm} + \hat{\imath}_{Lm})}{dt} = V_{in} + \hat{v}_{in} - (V_{Cc} + \hat{v}_{Cc})(1 - D - \hat{d}) \\ L_m \dfrac{d(I_{Lm} + \hat{\imath}_{Lm})}{dt} = -\dfrac{(1 - D - \hat{d})(V_{cm} + \hat{v}_{cm})}{(N+1)} \\ \quad + \dfrac{\left(1 + N(D + \hat{d})\right)(V_{in} + \hat{v}_{in})}{(N+1)} \\ C_c \dfrac{d(V_{Cc} + \hat{v}_{Cc})}{dt} = \dfrac{(I_{Lm} + \hat{\imath}_{Lm})(1 - D - \hat{d})}{N(D + \hat{d})} \\ \quad - \dfrac{(V_{in} + \hat{v}_{in}) \cdot (N+2)^2 \cdot (N+1)}{N\left((D + \hat{d}) \cdot R_o + (N + (D + \hat{d})N)\, NL_K\right)} \\ C_m \dfrac{d(V_{Cm} + \hat{v}_{Cm})}{dt} = \dfrac{(I_{Lm} + \hat{\imath}_{Lm})(1 - D - \hat{d})}{(N+1)} \\ \quad - \dfrac{(I_{Lm} + \hat{\imath}_{Lm})(D + \hat{d})}{N} \\ C_o \left\langle \dfrac{d(V_o + \hat{v}_o)}{dt} \right\rangle = -\dfrac{(V_{in} + \hat{v}_{in})(N+2)}{NL_K} \\ + \dfrac{(NL_K(N + (D + \hat{d})N) + (D + \hat{d})R_o)(1 - D - \hat{d})(V_o + \hat{v}_o)}{NL_K R_o (D + \hat{d})} \end{cases} \tag{14}$$

Equation (14) is linearized about the nominal equilibrium point by expanding and neglecting the higher order perturbation terms, then removing the steady-state quantities gives the small signal ac model of the converter. Then, by taking the Laplace transform the following equation results

$$\begin{cases} s \cdot L_m \cdot \hat{\imath}_{Lm}(s) = \hat{v}_{in}(s) - V_{Cc}\hat{d}(s) + (1 - D)\hat{v}_{Cc}(s) \\ s \cdot L_m \cdot \hat{\imath}_{Lm}(s) = -\dfrac{(1 - D)\hat{v}_{Cm}(s)}{(N+1)} + \dfrac{(NV_{in} - V_{Cm})(s)}{(N+1)} \\ \quad + \dfrac{(1 + ND)\hat{v}_{in}(s)}{(N+1)} \\ s \cdot C_c \cdot \hat{v}_{Cc}(s) = \dfrac{(1 - D)\hat{\imath}_{Lm}(s)}{ND} + \dfrac{(N+2)^2 \cdot (N+1)\hat{v}_{in}(s)}{NL_K(N + ND) + NDR_o} \\ s \cdot C_m \cdot \hat{v}_{Cm}(s) = \dfrac{(N - D - 2ND)\hat{\imath}_{Lm}(s)}{N(N+1)} - \dfrac{I_{Lm}\hat{d}(s)}{(N+1)} - \dfrac{I_{Lm}\hat{d}(s)}{N} \\ s \cdot C_o \cdot \hat{v}_o(s) = -\dfrac{(N+2)\hat{v}_{in}(s)}{NL_K} + \dfrac{(N^2 L_K + R_o)V_o\hat{d}(s)}{NL_K R_o} \\ \quad \dfrac{(NL_K(N + ND) + DR_o)(1 - D)\hat{v}_o(s)}{NL_K R_o D} \end{cases} \tag{15}$$

From (15) various transfer functions can be developed suitable for closed loop control system design of the converter such as control to output (16), control to magnetizing inductor current (17) and output voltage to current (18) transfer functions

$$G_{vd}(s) = \frac{\hat{v}_o(s)}{\hat{d}(s)} = \frac{1}{|A(s)|}[A_{51} \quad \cdots \quad A_{55}]\begin{bmatrix} b_1 \\ \vdots \\ b_5 \end{bmatrix} \tag{16}$$

$$G_{id}(s) = \frac{\hat{\imath}_{Lm}(s)}{\hat{d}(s)} = \frac{1}{|A(s)|}[A_{11} \quad \cdots \quad A_{15}]\begin{bmatrix} b_1 \\ \vdots \\ b_5 \end{bmatrix} \tag{17}$$

$$G_{vi}(s) = \frac{\hat{v}_o(s)}{\hat{\imath}_{Lm}(s)} = \frac{\hat{v}_o(s)}{\hat{d}(s)} \cdot \frac{\hat{d}(s)}{\hat{\imath}_{lm}(s)} \tag{18}$$

The control-to-output transfer function describes a standard third order system and exhibit a non-minimum phase system, which is typical behavior of converters with boost or buck-boost characteristics.

C. Model Validation

The control-to-output transfer function in (16) is verified in simulation by perturbing duty cycle set point with sinusoids of different frequencies and stores the corresponding output voltage. A discrete point can be found from the frequency response that describes how the system responds to the magnitude and phase of the injected sinusoids. Therefore, the control-to-output transfer function can be estimated from the measured data. Fig. 2 illustrates the Bode plots of both the calculated and estimated response of the control-to-output transfer function. It is reasonable to conclude that a good agreement exist between the models. This means that the calculated model can be used for the real system frequency domain analysis and controller design. The parameters used in the simulation and that of the calculated model are those listed in Table I.

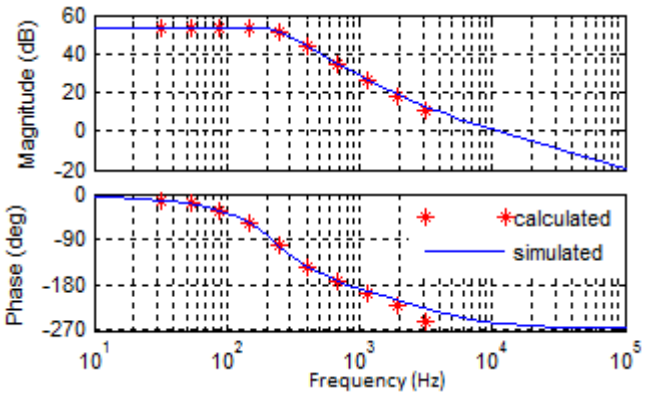

Fig. 2 Bode plots of model validation in Matlab

TABLE I. CONVERTER PARAMETERS

Parameter	Rating
Output Power (P_O)	250 W
Input Voltage (V_{in})	20 V
Output Voltage (V_O)	190 V
Switching Frequency (f_s)	50 KHz
Clamp capacitors (C_C)	4.7 µF
Switched Capacitor (C_m)	10 µF
Output capacitor (C_O)	50 µF
Turns Ratio (n_2/n_1)	1:1.8
Magnetizing Inductance (L_m)	82 µH

IV. CONTROLLER DESIGN

Fig. 3 illustrates the control strategy used to investigate the closed loop dynamic performance of the converter. It is a typical dual loop control, comprising of inner current loop and outer voltage loop. The presence of the right half plane (RHP) zero in the control-to-output transfer function of converters with boost or buck-boost characteristics tends to destabilize the traditional single-loop feedback control. It is difficult to

obtain an adequate phase margin (PM), because during transient the phase lag of the right (RHP) zero causes the output to change initially in the wrong direction [15].

The primary goal is to regulate the converter output voltage.The output voltage changes as the load shift and the detected feedback signal are processed via a proportional-integral (PI) controller. The outer voltage loop provides the reference signal of the inner current loop, and this reference is compared with the measured input current, and the error is processed via the inner current loop PI controller. The loops are usually defined to satisfy certain design criteria of PM and bandwidth. The duty cycle value is determined by the inner current control loop. The outer voltage loop has slow dynamics whilst the inner current loop has fast dynamics. This is to allow the input current to respond more quickly than the converter output voltage. Using the transfer functions presented in (17) and (18), the dual loop controller can be designed, using the average current mode control method [15].

Fig. 4 shows the block diagram of the current mode control structure in continuous domain. The padè approximation block and a static gain represents the converter pulse width modulation (PWM) module [16].

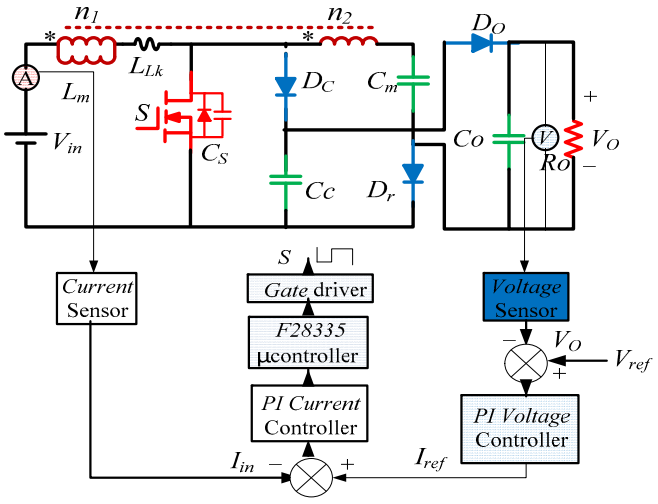

Fig. 3 Control diagram of dual loop control architecture

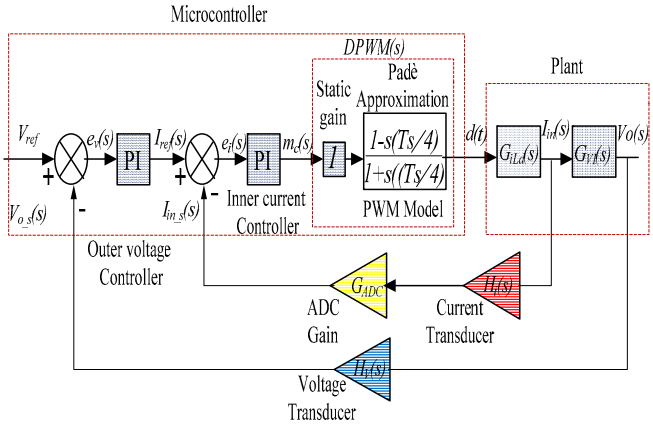

Fig. 4 Block diagram of current mode control

A. *Innerr Current Control Loop*

Using the block diagram in Fig. 4, the inner current PI controller is designed first, using the control to duty cycle transfer function of (17), whose Bode diagram is shown in Fig.5.The open loop transfer function of the inner current control loop (simply a cascade connection of all blocks) is required to design the controller. This transfer function is given by

$$G_{oL}(s) = \frac{K_p(s + K_i/K_p)}{s} \cdot \frac{(1 - s\,T_s/4)}{(1 + s\,T_s/4)} \cdot H_i(s) \cdot G_{id}(s) \qquad (19)$$

where $H_i(s)$ is the current sensor gain. The continuous time system in (17) is first discretized with zero order hold (ZOH) given by

$$G_{id}(z) = Z\{\frac{1}{s}(1 - e^{-sTs})H(s) \cdot G_{id}(s)\} \qquad (20)$$

Once this is available, the digital PI controller is designed directly in the discrete time domain using methods similar to continuous time frequency response. The compensator design is driven by certain specifications concerning the closed loop performance (such as speed of response or tracking error with respect to the reference signal). For this reason, a closed loop bandwidth f_{CL} of one tenth of the switching frequency f_s is intended to be achieved with at least phase margin PM of 60^o. The subsequent step is to determine the proportional gain K_p and integral gain K_I that guarantee compliance with these specifications.

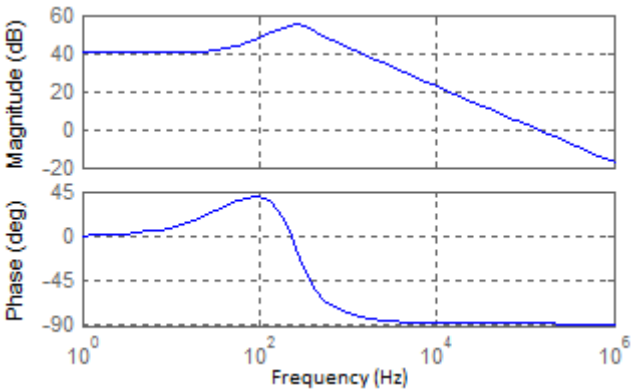

Fig. 5 Control to duty cycle transfer function Bode diagram

The controller is designed in Matlab using a "sisotool" graphical user interface based on Zeigler-Nichols tuning that allows the closed loop frequency response to be interactively changed by modifying the pole-zero location of the PI compensator. The corresponding feedback compensator gains from the same interface are $K_p = 0.011$ and $K_I T_s = 0.00005$ respectively.

B. *Outer Voltage Loop*

The outer voltage PI controller is design in similar way using the voltage to current transfer function (18), the Bode diagram is shown in Fig. 6. As previously explained , the outer voltage loop has slow dynamics, this is done to consider the inner current control loop as having a unitary gain and zero

phase when designing the outer voltage loop. The open loop gain is

$$G_{oL}(s) = \frac{K_p(s + K_i/K_p)}{s} \cdot H_v(s) \cdot G_{vi}(s) \qquad (21)$$

where $H_v(s)$ is the voltage transducer gain. To ensure sufficient stability around equilibrium point due to parameter variation influence, a closed loop bandwidth f_{CL} of one tenth of the inner current loop is intended to be achieved with at least phase margin PM of 60^o. Following the same method described in the current loop the proportional gain K_p and integral gain K_I of the voltage loop that guarantees compliance with these specifications are $K_p = 0.7$ and $K_I T_s = 0.0019$ respectively.

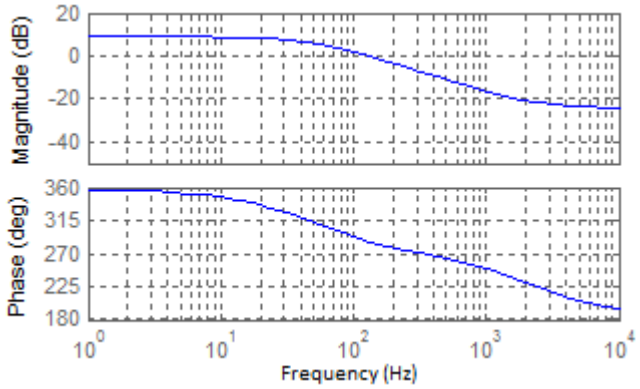

Fig. 6 Bode diagram of voltage to current transfer function

V. Experimental Validation

To verify the theoretical analysis and the closed loop dynamics performance of the converter. A 250W prototype is considered here and its parameters are listed in Table I. The input current of the converter and output voltage is measured by sampling the signal from the respective sensors synchronized with the apex of the PWM carrier signal. The control routines are implemented digitally in real time via TMS320F28335 digital signal processor. The transient response characteristics such as settling time, peak over shoot and steady state error for output voltage regulation during the load perturbation are observed. The measured experimental result of the load disturbance cases are demonstrated in Fig. 7 and 8

In Fig. 7, a step change in load resistance is applied, causing a step decrement in output power from 250 W to 125 W and vice versa at fixed input voltage of 20 V. The results clearly show that the desired output voltage is well regulated, with zero steady state error. Likewise, at the point of a load change, there is no overshoot or undershoot in the output voltage waveform. The output current settles at the next steady-state value due to duty ratio adjustment to regulate the converter output voltage. Another load disturbance is applied in Fig. 8, causing a step decrement in output power from full load to no load and vice versa. Once more, the dynamic characteristics indicate that the output voltage stays constant, with zero steady state error. Note that for all these perturbation cases the output voltage is insensitive to the disturbance, due to the performance of the controllers.

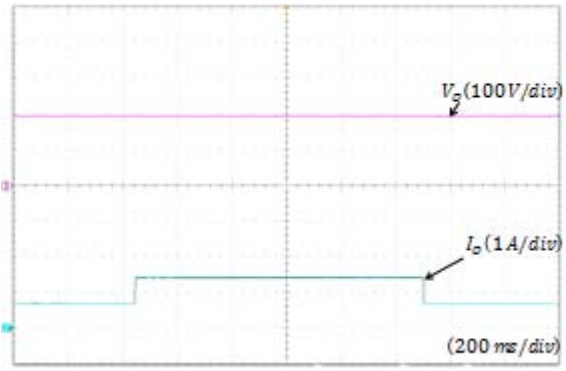

Fig. 7 Step change in load from half load to full load

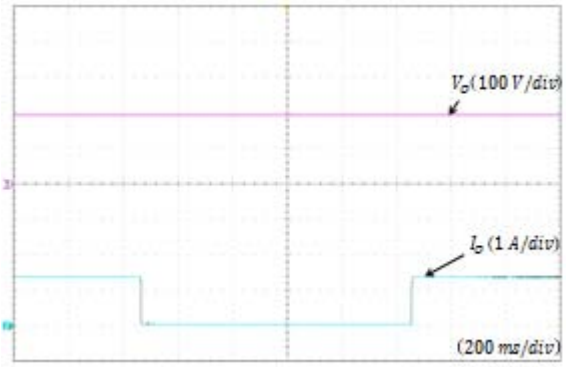

Fig. 8 Load change from full load to no load

VI. Conclusion

The derivation of the small signal model of a high step-up converter with coupled inductor and switched capacitor in CCM is presented in this paper. The derived model is validated in simulation and used in the design of the controllers. The dynamic response of the converter under the influence of the designed PI controller is verified via an experimental laboratory prototype converter. The proposed converter exhibits high performance, high gain operation. It is a beneficial alternative to the conventional boost converter in many industrial applications.

References

[1] Elgendy MA, Atkinson DJ, Zahawi B. Experimental Investigation of the Incremental Conductance MPPT Algorithm at High Perturbation rates. IET Renewable Power Generation 2016, **10**(2), 133-139.

[2] Elgendy MA, Atkinson DJ, Zahawi B, Giaouris D. Dynamic Behaviour of DC Motor-Based Photovoltaic Pumping Systems under Searching MPPT Algorithms. IEEE International Conference on Power Engineering, Energy and Electrical Drives, POWERENG 2009, Lisbon, Portugal, 18-20 March 2009.

[3] Elgendy MA. Comparative investigation on hill climbing MPPT algorithms at high perturbation rates. IEEE International Renewable Energy Congress IREC 2016, Hammamet, Tunisia, 21-23 March 2016.

[4] Armstrong M, Atkinson DJ, Johnson CM, Abeyasekera TD. Auto-calibrating dc link current sensing technique for transformerless, grid connected, H-bridge inverter systems. IEEE Trans. Power electron., vol. 21, no. 5, p. 1385-1393, Sept.2006.

[5] Armstrong M, Atkinson DJ, Johnson CM, Abeyasekera TD. Low order harmonic cancellation in a grid connected multiple inverter system via

current control parameter randomization. IEEE Trans. Power Electron. vol. **20, no.** 4, p. 885-892, Jul. 2005.

[6] Abdelali El Aroudi, Damian Giaouris, Herbert Ho-Ching Iu, Ian A Hiskens. A Review on Stability Analysis Methods for Switching Mode Power Converters. IEEE Journal of Emerging and Selected Topics in Circuits and Systems., vol. 5, no. 3, p. 302-315, Sept.2015.

[7] Giaouris D, Stergiopoulos F, Ziogou C, Ipsakis D, Banerjee S, Zahawi B, Pickert V, Voutetakis S, Papadopoulou S. Nonlinear Stability Analysis and a New Design Methodology for a PEM Fuel Cell Fed DC-DC Boost Converter. Int. Journal of Hydrogen Energy, vol. 37, no. 23, p.18205-18215. Dec.2012.

[8] Haimin, T., J.L. Duarte, and M.A.M. Hendrix, Line-Interactive UPS Using a Fuel Cell as the Primary Source. IEEE Trans. Indust. Electron, vol.**55, no.**8, p. 3012-3021, Aug,2008

[9] Lambert SM, Pickert V, Atkinson DJ, Zhan H. Transformer based equalisation circuit applied to n-number of high capacitance cells. IEEE Trans. Power electron., vol.31**, no.**2, p. 1334-1343, Feb,2016

[10] James P, Forsyth A, Calderon-Lopez G, Pickert V. DC-DC converter for hybrid and all electric vehicles. In: The 24th International Battery, Hybrid and Fuel Cell Electric Vehicle Symposium and Exhibition (EVS 2009). 2009, Stavanger, Norway.

[11] Zbede YB, Gadoue SM, Atkinson DJ. "Model Predictive MRAS Estimator for Sensorless Induction Motor Drives". IEEE Trans. Ind. Electron., vol. 63, no. 6, pp. 3511–3521, (2016).

[12] Muhammad, M., M. Armstrong, and M. Elgendy, "Non-isolated, high gain, boost converter for power electronic applications",, in Proc. of 8th IET International Conference on Power Electronics, Machines and Drives.Glasgow,Scotland,UK.Jan.2016.pp1-6

[13] Muhammad, M., M. Armstrong, and M. Elgendy, "Non-isolated DC-DC converter for high step-up ratio Applications", in Proc. Power Electronics and Applications (EPE'15 ECCE-Europe), 17th European Conference on. Geneva, Switzerland Sept. 2015.pp.1-10

[14] Muhammad, M., M. Armstrong, and M. Elgendy, "A Non-isolated Interleaved Boost Converter for High Voltage Gain Applications". IEEE Journal of Emerging and Selected Topics in Power Electronics, **vol.** 4 no 2, pp. 352-362, Jun. 2016.

[15] R. W. Erickson and D. Maskimovic, Fundamentals of Power Electronics. USA: Springer, 2000.

[16] S. Buso and P.Matavelli, Digital Control in Power Electronics. USA: Morgan & Claypool, 2006